

Photophysical properties, complexometry, and aggregation-induced emission of a 2-donor-substituted 3-ethynylquinoxaline

Narges Irani, Simon Höwedes, Franziska K. Merkt-Tasch, and Thomas J. J. Müller*

Heinrich-Heine-Universität Düsseldorf, Mathematisch-Naturwissenschaftliche Fakultät, Institut für Organische Chemie und Makromolekulare Chemie Universitätsstrasse 1, D-40225 Düsseldorf, Germany

E-mail: ThomasJJ.Mueller@uni-duesseldorf.de

Dedicated to Prof. Dr. Alan Aitken on the occasion of his 65th birthday

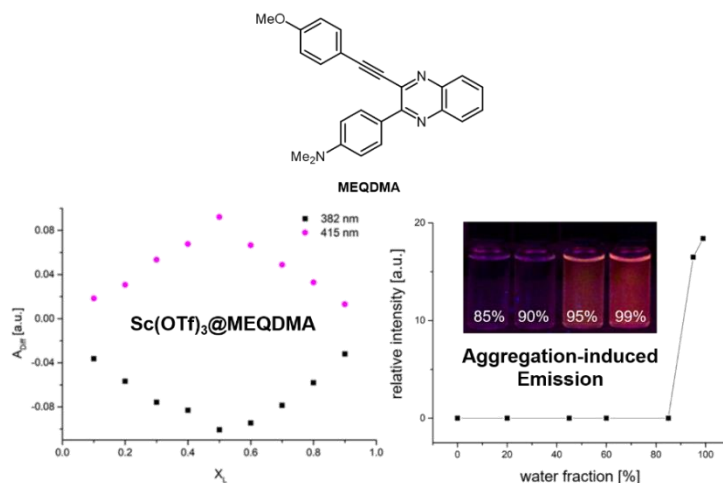
Received 11-13-2023

Accepted Manuscript 02-06-2024

Published on line 02-14-2024

Abstract

4-(3-((4-Methoxyphenyl)ethynyl)quinoxalin-2-yl)-*N,N*-dimethylaniline (**MEQDMA**) shows intense solid-state luminescence. As related derivatives **MEQDMA** is highly emission solvatochromic with considerable redshifted emission in polar solvents and a large change of dipole moment according to Lippert-Mataga analysis. A UV/Vis screening with several mono-, di- and trivalent metal triflates reveals complexation with scandium and aluminium triflate. The former is characterized by Job plots, forming a 1:1 M:L complex with a complex formation constant $K_{ML} = 2700 \text{ L}^2 \cdot \text{mol}^{-1}$. In addition, **MEQDMA** also emits upon induced aggregation in binary acetonitrile/water or isopropanol/ water solutions at higher water content.

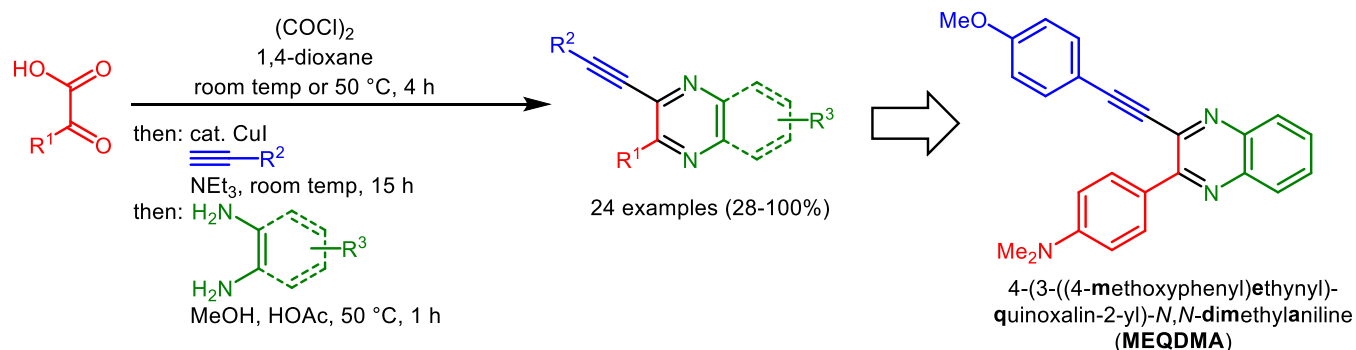


Keywords: Aggregation-induced emission – complexometry – donor-acceptor dyes – fluorescence– Job plots – quinoxalines

Introduction

Quinoxaline, the venerable formal benzopyrazine, has become an evergreen among bicyclic heterocycles with two nitrogen atoms.¹ Numerous quinoxaline derivatives have been reported to be highly biologically active^{2,3} and their potential in medicinal chemistry⁴ ranges from antiviral⁵ to anti-cancer agents.^{6,7} Electronically, quinoxaline can be considered to be strongly electron deficient as a consequence of its very weak basicity with a pK_b of 0.60 in water at 20 °C.⁸ Therefore, in the past decade, quinoxalines have increasingly found interest as constituents of functional dyes, in particular, as luminophores,⁹ solar cell dyes,¹⁰ TADF (thermally activated delayed fluorescence) emitters,¹¹ as chromogenic and fluorogenic cation¹² and anion sensors,¹³ as well as emitters upon induced aggregation, known as aggregation-induced emission (AIE), and due to their solvatochromic behavior.¹⁴ As a consequence of the ongoing interest in quinoxaline derivatives their syntheses have been constantly developed^{15,16} exploring novel modes of reactivity¹⁷ and also conceptual approaches by one-pot and multicomponent methodologies.¹⁸

In recent years, we have developed a consecutive multicomponent access to 2-(hetero)aryl 3-alkynyl quinoxalines by glyoxylation-alkynylation-cyclocondensation (GACC)¹⁹ and by consecutive three-component activation-alkynylation-cyclocondensation (AACC)²⁰ sequences. The latter sets out from (hetero)aryl glyoxylic acids via oxalyl chloride activation to give the (hetero)aryl glyoxylchlorides, which are alkynylated by copper catalysis in the same reaction vessel to give ynediones²¹ that are immediately cyclocondensed with *ortho*-phenylene diamines in a Hinsberg cyclization to give 2-(hetero)aryl 3-alkynyl quinoxalines in moderate to excellent yield in a one-pot process (Scheme 1). In addition, 3-alkynyl quinoxalines^{22,23} and also expanded derivatives like 3-aminovinylquinoxalines^{24,25} and 3-triazolylquinoxalines²⁶ display peculiar emission solvatochromicity and AIE characteristics.



Scheme 1. Consecutive three-component activation-alkynylation-cyclocondensation (AACC) synthesis of 2-(hetero)aryl substituted 3-ethynyl quinoxalines.

The AACC sequence provided 4-(3-((4-methoxyphenyl)ethynyl)quinoxalin-2-yl)-*N,N*-dimethylaniline (**MEQDMA**),²⁰ an orange solid that fluoresces intensively under the handheld UV-lamp. Therefore, we set out to study absorption and emission characteristics of **MEQDMA** in more detail. In particular, we report here on the complexation behavior of this *bis* donor-substituted quinoxaline **MEQDMA** and its AIE characteristics.

Results and Discussion

Compound **MEQDMA** was previously synthesized according to the consecutive three-component AACCC synthesis and obtained as an analytical pure orange solid compound in 60% yield after chromatographic purification.²⁰ The absorption and emission maxima were determined by UV/Vis and fluorescence spectroscopy in dichloromethane solutions at $c(\text{MEQDMA}) = 10^{-4}$ M (absorption) and $c(\text{MEQDMA}) = 10^{-7}$ M (emission) together with the molar decadic absorption coefficient ε , assuming and verifying the validity of Lambert-Beer law, and the fluorescence quantum yield Φ_F , determined by the relative method²⁷ with 4-(dicyanomethylene)-2-methyl-6-(*p*-dimethylaminostyryl)-4*H*-pyran (DCM) as a standard in methanol ($\Phi_F = 0.44$)²⁸ as well as the Stokes shift (Table 1, Figure 1).

Table 1. Absorption and emission maxima $\lambda_{\text{max,abs}}$ and $\lambda_{\text{max,em}}$, of compound **MEQDMA**, decadic molar absorption coefficient ε , fluorescence quantum yield, and Stokes shift $\Delta\tilde{\nu}$ (recorded in dichloromethane, $T = 298$ K)

$\lambda_{\text{max,abs}}$ [nm] ^[a] (ε [L·mol ⁻¹ ·cm ⁻¹])	$\lambda_{\text{max,em}}$ [nm] ^[b] (Φ_F)	Stokes shift $\Delta\tilde{\nu}$ [cm ⁻¹] ^[c]
268.5 (27600), 280 (26700), 312 (29800), 340 (29200), 413 (11500)	588 (0.43) ^[d]	7200

[a] Recorded in CH₂Cl₂, $c(\text{MEQDMA}) = 10^{-4}$ M at $T = 298$ K. [b] Recorded in CH₂Cl₂, $c(\text{MEQDMA}) = 10^{-7}$ M at $T = 298$ K. [c] $\Delta\tilde{\nu} = 1/\lambda_{\text{max,abs}} - 1/\lambda_{\text{max,em}}$. [d] The quantum yield was determined according to the relative method ($\pm 10\%$)²⁷ with (DCM) as a standard in methanol ($\Phi_F = 0.44$).²⁸

Dye **MEQDMA** revealed five absorption maxima at 268.5, 280, 312, 340, and 413 nm in dichloromethane, where the longest wavelength maximum displays the lowest decadic molar absorption coefficient. Upon excitation at this longest wavelength absorption maximum an intense emission at 588 nm with a quantum yield of 0.43 was found. This accounted to a quite large Stokes shift of 7200 cm⁻¹.

Already to the naked eye a positive emission solvatochromicity of dye **MEQDMA** could be seen by increasing the solvent polarity (Figure 2). According to solvent polarity dependent absorption spectroscopy the longest wavelength maximum was determined in a narrow range from 404 (cyclohexane) to 420 nm (methanol). However, emission maxima spanned a range from 477 nm (cyclohexane) to 680 nm (acetonitrile) and emission color ranged from sky blue to deep purple (Figure 3, Table 2).

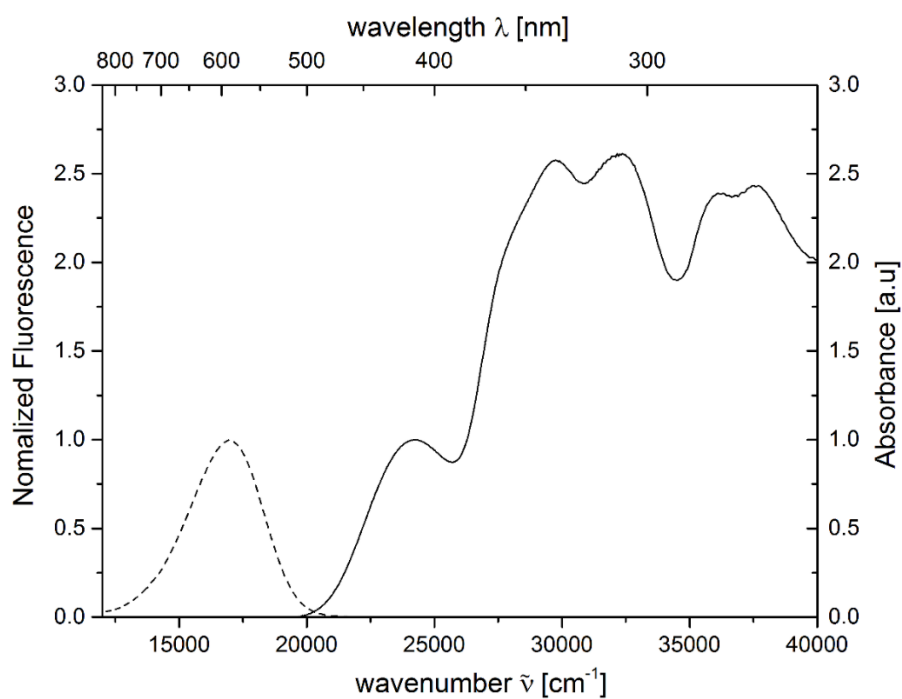


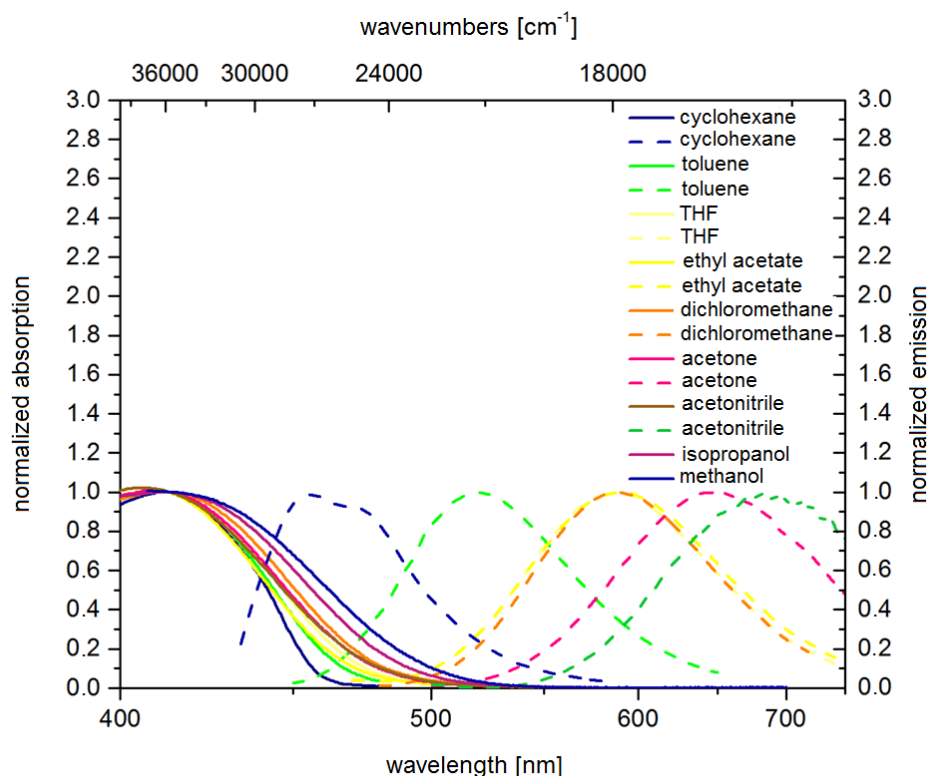
Figure 1. Absorption (solid line) and emission spectra (dashed line, normalized to the longest wavelength absorption band) of compound **MEQDMA** (recorded in dichloromethane at $T = 298$ K, absorption: $c(\text{MEQDMA}) = 10^{-4}$ M, emission: $c(\text{MEQDMA}) = 10^{-7}$ M).



Figure 2. Dye **MEQDMA** ($c(\text{MEQDMA}) = 10^{-4}$ M, $T = 293$ K) in daylight (top) and fluorescence (bottom) with variable solvent polarity (from left to right: cyclohexane, toluene, tetrahydrofuran, ethyl acetate, dichloromethane; acetone, acetonitrile, isopropanol, methanol; $\lambda_{exc} = 365$ nm, hand-held UV lamp).

Table 2. Selected absorption and emission maxima, decadic molar absorption coefficients ε , Stokes shifts $\Delta\tilde{\nu}$, orientation polarizability Δf , and $E_T(30)$ values of **MEQDMA**

solvent	$\lambda_{\max,abs}$ [nm] (ε [L·mol ⁻¹ ·L ⁻¹])	$\lambda_{\max,em}$ [nm]	$\Delta\tilde{\nu}$ [cm ⁻¹]	Δf	$E_T(30)^{29}$ [kcal·mol ⁻¹]
cyclohexane	404 (5120)	477	3700	0.00	30.9
toluene	412 (6103)	520	5040	0.02	34.7
tetrahydrofuran	410 (2556)	589	7410	0.18	37.4
ethyl acetate	407 (4433)	589	7590	0.20	38.1
dichloromethane	412 (3146)	590	7320	0.21	40.7
acetone	410 (3156)	643	8840	0.28	42.2
acetonitrile	408 (4393)	680	9800	0.31	45.6
isopropanol	415 (4523)	–	–	0.28	48.4
methanol	420 (3035)	–	–	0.31	55.4

**Figure 3.** UV/vis absorption (solid lines) and emission spectra (dashed lines) of compound **MEQDMA**, measured in nine solvents of different polarity (recorded at $T = 293$ K).

This pronounced emission solvatochromicity, which is typical for the class of 2-(hetero)aryl-3-ethynyl quinoxalines, has been rationalized by TDDFT calculations for some representatives,^{19,20,23} and has a consequence for the intense charge transfer transition of the longest wavelength absorption band and the polar vibrationally relaxed excited S_1 state. While a plot of the emission maxima against the $E_T(30)$ values of the Reichardt scale²⁹ already semiquantitatively supported the positive emission solvatochromicity, the Lippert-Mataga model^{30,31} allowed for estimating the change of dipole moment by plotting the Stokes shifts $\Delta\tilde{\nu}$ against

the orientation polarizability Δf (for details, see Supp Inf). The Lippert plot for dye **MEQDMA** gave a very good linear correlation ($r^2 = 0.97$) (Figure 4).

According to equation 1

$$\Delta f = \frac{\varepsilon_r - 1}{2\varepsilon_r + 1} - \frac{n^2 - 1}{2n^2 + 1} \quad (1)$$

the orientation polarizability Δf was calculated from the relative permittivity ε_r and the optical refractive index n of the respective solvent.³²

The excellent linear correlation of the Stokes shift $\Delta\tilde{\nu}$ with the Lippert-Mataga polarity parameters Δf (ε_r, n) indicated the dominant importance of a general solvent effect. The change in dipole moment from the electronic ground to the vibrationally relaxed excited state was calculated according to the Lippert-Mataga equation (equation 2).

$$\tilde{\nu}_a - \tilde{\nu}_f = \frac{2\Delta f}{hca^3} (\mu_E - \mu_G)^2 + const \quad (2)$$

While $\Delta\tilde{\nu}_a$ and $\Delta\tilde{\nu}_f$ represent the absorption and emission maxima (in m^{-1}), μ_E and μ_G are the dipole moments in the excited and ground state (in Cm), ε_0 (8.8542×10^{-12} As $\text{V}^{-1} \text{m}^{-1}$) is the vacuum permittivity constant, h (6.6256×10^{-34} J s) is Planck's constant, c (2.9979×10^8 ms^{-1}) is the speed of light, and a is the radius of the solvent cavity occupied by the molecule (in m).

Assuming a spherical dipole, the Onsager radius a , which was used to approximate the molecular volume of the molecule in solution, was estimated from the optimized ground-state structure of compound **MEQDMA** obtained from DFT calculations in dichloromethane as an implicit solvent dielectric (CAM-B3LYP functional, 6 311+G (d, p) basis set). Employing a value of 6.03 Å ($6.03 \cdot 10^{-10}$ m), the change in dipole moment $\Delta\mu$ was calculated to 17.83 D ($5.95 \cdot 10^{-29}$ Cm). This large value supports a pronounced charge separation upon charge transfer excitation.

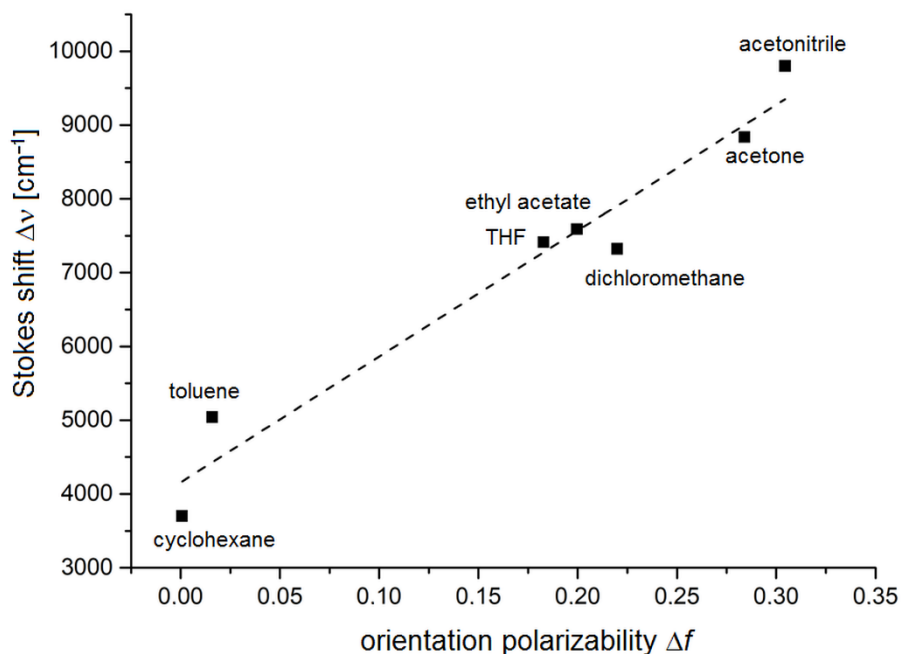


Figure 4. Lippert plot (Stokes shift $\Delta\tilde{\nu}$ as a function of orientation polarizability Δf) for dye **MEQDMA** ($n = 7$, $r^2 = 0.97$).

The presence of two basic quinoxaline nitrogen atoms in **MEQDMA** suggests halochromicity of the underlying chromophore. Indeed, monoprotonation of a dichloromethane solution of **MEQDMA** proceeded via several isosbestic points. The titration plot of **MEQDMA** with trifluoroacetic acid (TFA) gave a pK_a of 2.91 for the monoprotonated chromophore **MEQDMA-H⁺**, i.e. it is about 2.3 orders of magnitude less acidic than the parent compound quinoxaline ($pK_a = 0.6$).⁸ Upon protonation the fluorescence signal was quenched (see Supp Inf) and employing Stern-Vollmer analysis for a static quenching the obtained Stern-Vollmer constant K_{SV} was interpreted as the K_a of the protonated dye **MEQDMA-H⁺**. The Stern-Vollmer titration of **MEQDMA** thereby furnished a pK_a of 3.1, i.e. quite similar to the a pK_a from absorption spectroscopy titration.

Encouraged by the significant halochromicity we next assumed that dye **MEQDMA** with Lewis basic nitrogen atoms also could reveal metallochromicity. A quick screening for the changes of the longest wavelength absorption band in the absorption spectra of **MEQDMA** in acetonitrile (Figure 5A) and ethyl acetate (Figure 5B) in the presence of sodium, potassium, silver, magnesium, calcium, aluminium, scandium, silver, nickel, and copper triflate revealed that only aluminium, copper, scandium and magnesium triflate caused considerable changes of the spectra indicating complexation of **MEQDMA** by these metal ions (Table 3).

Table 3. Screening of metallochromicity by selected absorption maxima $\lambda_{max,abs}$ of dichloromethane solutions of **MEQDMA** and in the presence of metal triflates in acetonitrile and ethyl acetate at $T = 293$ K (only absorption maxima different from **MEQDMA** are given)

Ligand + metal triflate	$\lambda_{max,abs}$ [nm] in acetonitrile	$\lambda_{max,abs}$ [nm] in ethyl acetate
MEQDMA	407	407
MEQDMA + NaOTf	— ^a	— ^a
MEQDMA + KOTf	— ^a	— ^a
MEQDMA + AgOTf	— ^a	— ^a
MEQDMA + Mg(OTf) ₂	450	449
MEQDMA + Ca(OTf) ₂	— ^a	— ^a
MEQDMA + Al(OTf) ₃	450	378
MEQDMA + Sc(OTf) ₃	450	367
MEQDMA + AgOTf	— ^a	— ^a
MEQDMA + Ni(OTf) ₂	— ^a	— ^a
MEQDMA + Cu(OTf) ₂	365	305

^a No change to the absorption maximum of **MEQDMA** can be detected.

In acetonitrile only Cu(OTf)₂ caused a hypsochromic shift of the lowest energy band (365 nm) compared to the free ligand **MEQDMA** (407 nm), while Mg(OTf)₂, Al(OTf)₃, and Sc(OTf)₃, revealed a bathochromic complexation shift to 450 nm. Interestingly, in ethyl acetate the absorption maxima in the presence of Al(OTf)₃ (378 nm), Cu(OTf)₂ (305 nm), and Sc(OTf)₃ (367 nm) shifted hypsochromically to the free ligand **MEQDMA** (407 nm), however, in the presence of Mg(OTf)₂ a similar bathochromic shift (449 nm) was detected as in acetonitrile.

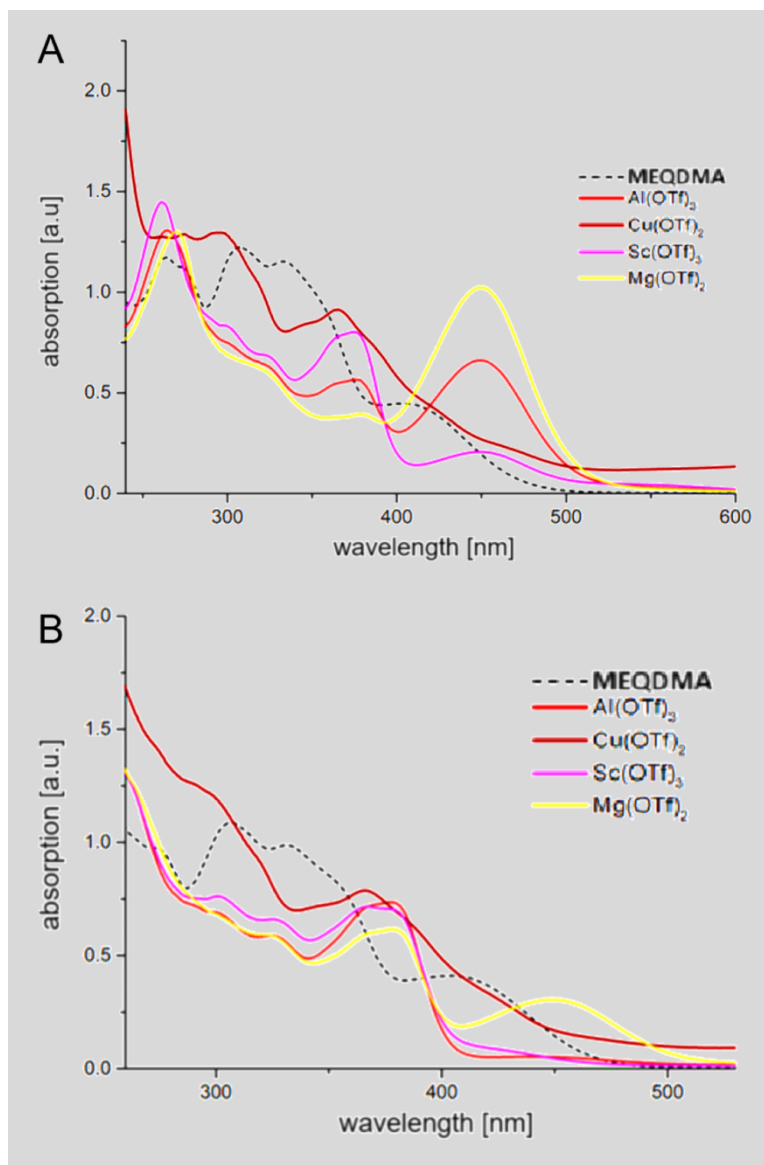


Figure 5. Absorption spectra of **MEQDMA** and in presence of Al(OTf)₃, Cu(OTf)₂, Sc(OTf)₃, and Mg(OTf)₂ in acetonitrile (A) and ethyl acetate (B) (recorded at $T = 293$ K, $c(\text{MEQDMA}) = 10^{-4}$ M).

Therefore, we became interested in the stoichiometry for complexation of Sc(OTf)₃ and **MEQDMA** in ethyl acetate. Complexation of a metal cation M and a ligand L involves an equilibrium between the free ligand, the metal cation, and the complex M_aL_b. For assessing the complex stability, first the complex stoichiometry has to be determined. The complexation constant results then from the mass action law.

The method of continuous variation (MCV), also called Job plot, provides qualitative and quantitative insight into complex stoichiometry. Using this method, the total volume and concentration of ligand L and metal cation M is kept constant and the relative ratio of M and L is varied.³³ For the Job plot method, the concentration of a complex M_aL_b is plotted against the mole fraction X_L of ligand or chromophore. The resulting maximum or minimum of this plot gives the ratio of the two components in the formed complex (parameters a and b). For the complex formation of two components L and M, the general equation 3 can be used.



For the Job plot experiment and the determination of complex stoichiometry, the spectra of the ligand-metal salt mixtures at different ratios at constant concentration are recorded. Difference spectra are generated according to equation 4,

$$A_{diff} = A_{obs} - A_L \quad (4)$$

where A_{obs} is the observed absorbance and A_L is the absorbance of the pure ligand.

The Job plots resulted from plotting the difference absorbances A_{diff} at the maximum at 384 nm (increase indicates formation of the ML complex) and at the minimum at 415 nm (decrease indicates consumption of the free ligand **MEQDMA**) against the mole fraction X_L (Figure 6).

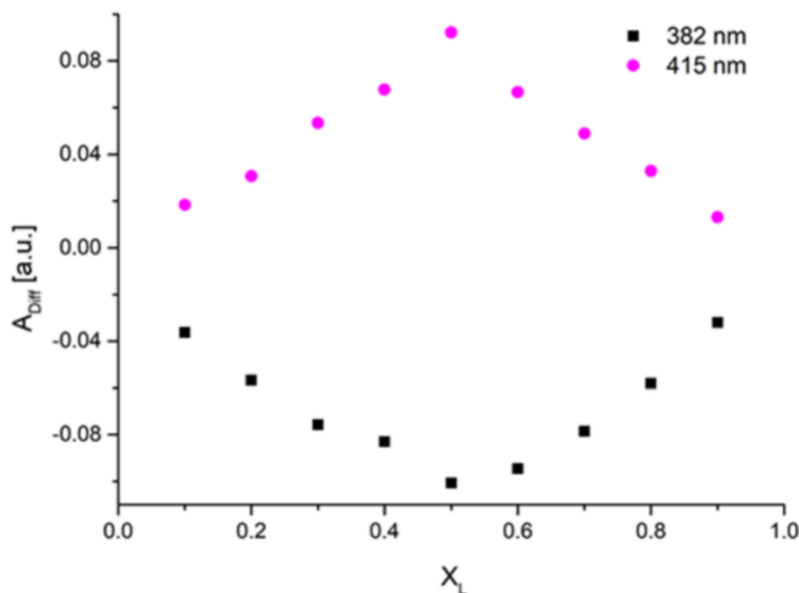


Figure 6. Job plots of **MEQDMA** and in presence of mole fractions X_L of $\text{Sc}(\text{OTf})_3$ in ethyl acetate (recorded at $T=293\text{ K}$).

Stable complexes were expected to have two linear subsegments intersecting at a point in the job plot.³⁴ Both the maximum of the plot at 415 nm and the minimum of the plot at 382 nm were at $X_L = 0.5$, indicating an equimolar stoichiometry of **MEQDMA** with $\text{Sc}(\text{OTf})_3$. However, the Job plot for the complexation of **MEQDMA** with $\text{Sc}(\text{OTf})_3$ in acetonitrile revealed a maximum and minimum at $X_L = 0.6$ (see Supp Inf). This suggested a 2:3 ratio of $\text{Sc}(\text{OTf})_3$ to **MEQDMA**, a rather unusual ratio for the Job plot method. It can be interpreted that in acetonitrile an ML_2 and an ML complex were simultaneously formed. However, if there is more than one complex the Job plot method becomes less reliable for determining the complex stoichiometry.^{35,36}

The complexation constant was used to describe the stability of the complex. Here, to determine the complexation constant, the concentration of **MEQDMA** was kept constant, while the concentration of $\text{Sc}(\text{OTf})_3$ was varied. For the determination of the complexation constant of **MEQDMA** with $\text{Sc}(\text{OTf})_3$ in ethyl acetate the occurrence of the isosbestic points in the absorption spectra clearly indicated that the complex formed without transitioning intermediates. Here, the titration curve displayed two isosbestic points at 362 and 393 nm, indicating an equilibrium between the free dye **MEQDMA** and the corresponding ML complex $\text{Sc}(\text{OTf})_3\text{@MEQDMA}$ that absorbs at 384 nm (Figure 7). This could be clearly seen in the difference spectra (see Supp Inf).

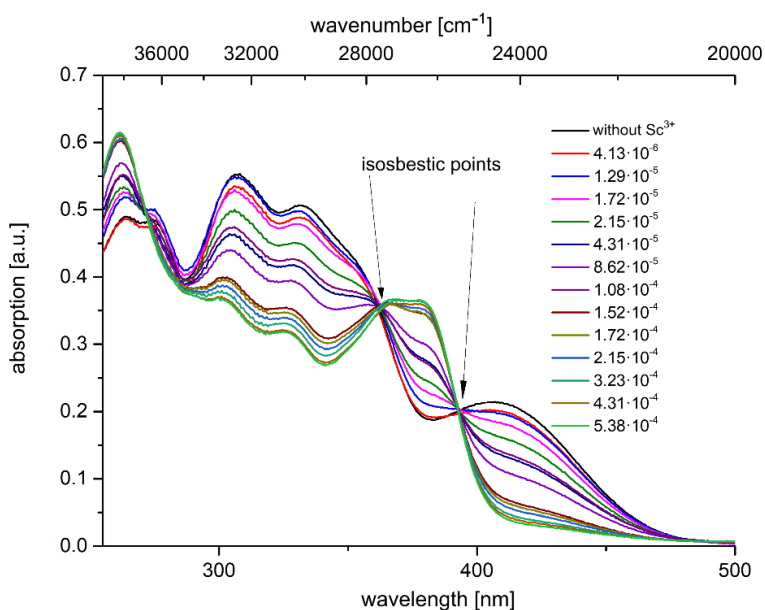


Figure 7. Absorption spectra of **MEQDMA** and various concentrations of $\text{Sc}(\text{OTf})_3$ in ethyl acetate ($c(\text{Sc}(\text{OTf})_3)$ [$\text{mol} \cdot \text{L}^{-1}$], recorded at $T = 293 \text{ K}$).

By plotting the absorption maxima at 384 nm and absorption minima at 415 nm against the increasing concentration of $\text{Sc}(\text{OTf})_3$, it was seen that the absorption did not change above a concentration of $c(\text{Sc}^{3+}) = 2.15 \cdot 10^{-4} \text{ M}$ (Figure 8). This suggests that the ML complex forms until saturation is reached. Evaluation of these experimental data by a multivariate functional analysis (MatLab)³⁷ furnished the complexation constant $K_{ML} = 2700 \text{ L}^2 \cdot \text{mol}^{-1}$ (ML = $\text{Sc}(\text{OTf})_3@ \text{MEQDMA}$).

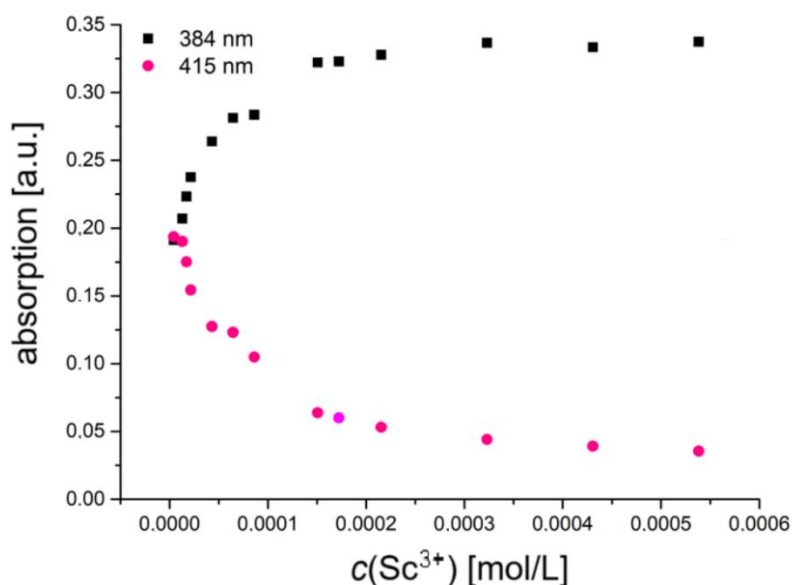


Figure 8. Plot of absorbance of $\text{Sc}(\text{OTf})_3@ \text{MEQDMA}$ (384 nm) and **MEQDMA** (415 nm) with increasing concentrations of $\text{Sc}(\text{OTf})_3$ in ethyl acetate.

Inspired by the extremely weak emission in more polar solvents (acetonitrile, isopropanol) and the solid-state emission of **MEQDMA** (vide supra) and the AIE behavior of expanded 5-(hetero)aryl-thien-2-yl substituted 3-ethynyl quinoxalines²² we set out to test the aggregation-induced emission characteristics of **MEQDMA**. While both in isopropanol and acetonitrile **MEQDMA** was only very weakly emissive, addition of water to a water content over 90 and 95%, respectively, induced aggregation and caused a significant increase of emission (Figures 9 and 10). Due to higher polarity of isopropanol the emission maximum of the aggregate appeared at 614 nm, whereas the maximum of the aggregates in acetonitrile appeared at 590 nm.

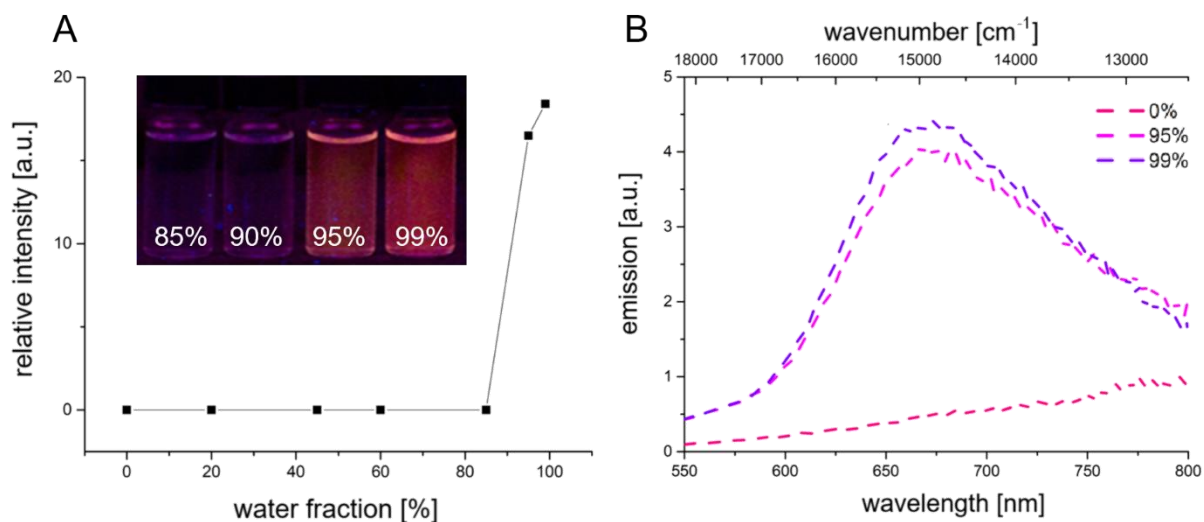


Figure 9. A: Emission intensity (inset: visualization of **MEQDMA** at 85, 90, 95 and 99% water content, $\lambda_{exc} = 365$ nm) and B: emission spectra (right) of **MEQDMA** in isopropanol/water mixtures upon increasing water content (recorded at $T = 298$ K, $c = 10^{-5}$ M, $\lambda_{exc} = 413$ nm).

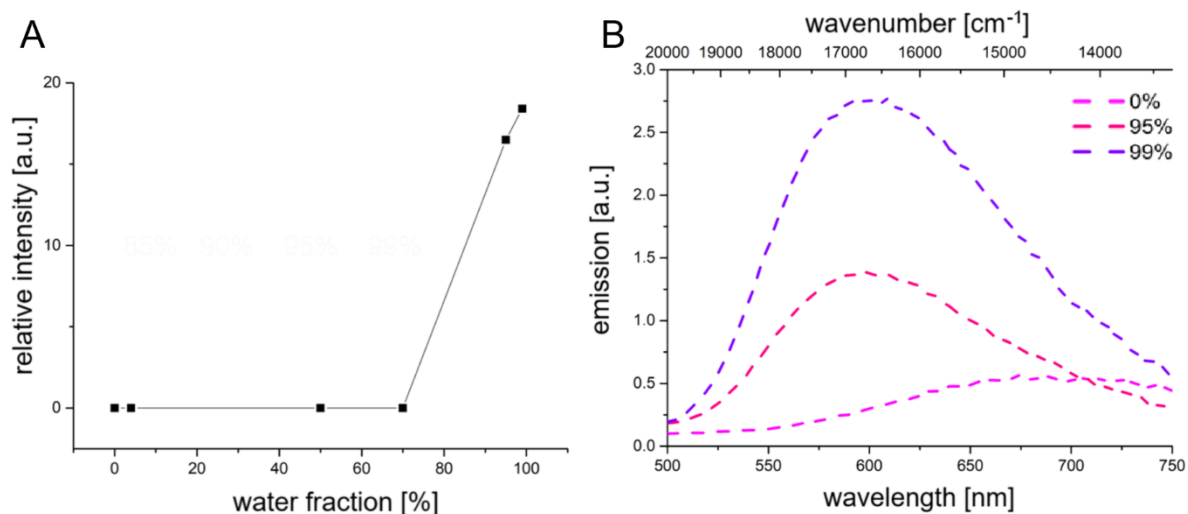


Figure 10. A: Emission intensity and B: emission spectra (right) of **MEQDMA** in acetonitrile/water mixtures upon increasing water content (recorded at $T = 298$ K, $c = 10^{-5}$ M, $\lambda_{exc} = 413$ nm).

Recording the fluorescence spectra of the solvent mixtures with a water content of 99% at different times after fresh preparation showed a decrease in fluorescence intensity. For the 99%water/acetonitrile mixture the emission disappeared after 40 min (Figure 11). For the 99%water/isopropanol mixture the decay to emission disappearance took 5 h. This can be interpreted that only particles of a certain size are emissive, whereas upon coagulation the emission intensity cause attenuation of the emission by self-absorbance. Apparently due to higher viscosity the coagulation in water-isopropanol is slower, which accounts for a longer stability of the aggregate particles.

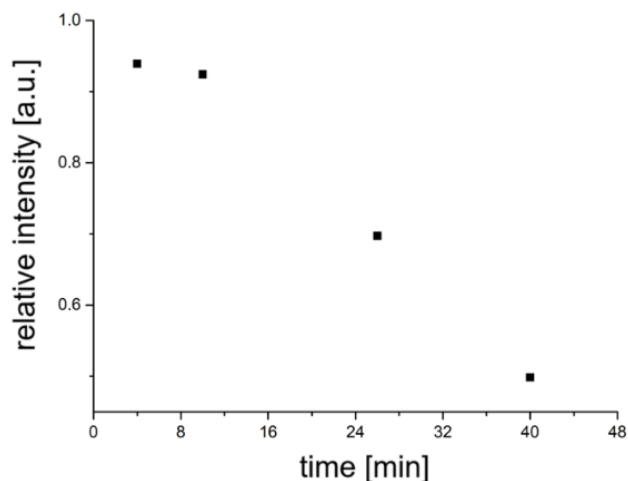


Figure 11. Time-dependent decrease of aggregate emission of **MEQDMA** in 99% water/acetonitrile mixture (recorded at $T = 298\text{ K}$, $c = 10^{-5}\text{ M}$, $\lambda_{exc} = 413\text{ nm}$).

Conclusions

The dye **MEQDMA** was constituted of a strong *p*-dimethylaminophenyl donor in 2-position and weaker donating *p*-anisylethynyl moiety in 3-position. As with almost all derivatives in the series of 3-ethynyl quinoxalines the title compound also displays strong solid-state emission and pronounced positive emission solvatochromicity with an impressive rainbow color-tuning. This accounts for an intense charge-transfer transition to a highly polar vibrationally relaxed excited state, which was assessed by a linear Lippert-Mataga plot and estimated to a change in dipole moment $\Delta\mu$ of 17.83 D. Moreover, **MEQDMA** also acts as a ligand for metal cations with some selectivity for $\text{Al}(\text{OTf})_3$, $\text{Cu}(\text{OTf})_2$, $\text{Sc}(\text{OTf})_3$, and $\text{Mg}(\text{OTf})_2$, where UV/Vis spectra clearly showed a change of the absorption characteristics upon complexation. For $\text{Sc}(\text{OTf})_3$, in ethyl acetate a Job plot accounted for a 1:1 stoichiometry which was ascertained by a titration to evaluate that the complex **Sc(OTf)₃@MEQDMA** was formed with a complexation constant K_{ML} of $2700\text{ L}^2 \cdot \text{mol}^{-1}$. Finally, as other strong donor-substitution in 2-position causes highly polarized chromophores amongst 3-ethynyl quinoxalines, we could additionally show that despite very weak emission, in acetonitrile and isopropanol aggregation was induced at high water contents. This aggregation-induced emission is highly intriguing at quite red shifted luminescence with a higher stability of aggregates in isopropanol/water toward coagulation. Further studies on related quinoxalines as multifunctional emissive sensors are currently underway.

Experimental Section

1. Instruments and Reagents

UV/Vis/NIR spectra were recorded on a Perkin Elmer Lambda 19 (Rev. 9B/9C) (Waltham/Massachusetts) and fluorescence spectra were recorded on a Perkin Elmer LS55 fluorescence spectrometer. The employed solvents (dichloromethane, acetonitrile, and ethyl acetate) were purchased HPLC-grade from *Merck Millipore* and used as received. Triflate salts were purchased from Sigma-Aldrich, ABCR, Acros Organics, Alfa Aesar, and Fluorochem and used as received. Trifluoroacetic acid was purchased from Reac Applichem.

2. Synthesis of MEQDMA

The synthesis of MEQDMA was previously reported²⁰ and the original analytically pure sample was used in this study.

3. Determination of the decadic molar absorption coefficients ε

A stock solution of **MEQDMA** was first prepared. **MEQDMA** (2 mg, 5 μmol) was dissolved in CH_2Cl_2 (25 mL) in a volumetric flask. From this stock solution, aliquots of 0.1, 0.3, 0.4, 0.5, and 0.7 mL were diluted with CH_2Cl_2 to a total volume of 3 mL in measuring flasks. At each of these five concentrations absorption spectra were recorded and the absorptions were plotted against the concentration. According to the Lambert-Beer's law the decadic molar absorption coefficients ε were determined for all absorption maxima.

λ_{max} [nm] (ε [$\text{L}\cdot\text{mol}^{-1}\cdot\text{cm}^{-1}$]) = 413 (11500), 340 (29200), 312 (29800), 280 (26700), 268.5 (27600).

4. Emission solvatochromicity of MEQDMA

Absorption and emission data of **MEQDMA** were recorded in solvents of different polarity and selected photophysical data (absorption and emission maxima, decadic molar absorption coefficients ε , Stokes shifts $\Delta\tilde{\nu}$, orientation polarizability Δf , and $E_{\tau}(30)$ values²⁹) are shown in Table 2.

5. Determination of the pKa of MEQDMA-H⁺

At TFA concentration between $7.32 \cdot 10^{-5}$ to $3.05 \cdot 10^{-3}$ M, assuming full ionization of TFA in CH_2Cl_2 the concentration of TFA was equal to the pH, the decrease of the non-protonated **MEQDMA** and the increase of the protonated species **MEQDMA-H⁺** was clearly detected. Based on the resulting isosbestic point, the $\text{p}K_a$ value of **MEQDMA-H⁺** was determined. The isosbestic point was indicative of equilibrium between the protonated and non-protonated species without involvement of an intermediate. The longitudinal wavelength absorption maximum ($\lambda_{\text{max}} = 340$ nm) was shifted to longer wavelengths ($\lambda_{\text{max}} = 385$ nm) with increasing protonation (Figure S1). From the unprotonated absorption spectrum and the protonated absorption spectra, the difference spectra were plotted. Based on the difference spectra, the positioning of two intense maxima and minima at 340 and 385 nm were determined (Figure S2).

The concentration of the TFA stock solution used in the titration experiment and the pH calculated as a result, as well as the corrected absorbances at the maximum (385 nm) and minimum (340 nm) were summarized in Table 4.

Table 4. Corrected absorbance of protonated and non-protonated **MEQDMA**, concentration of TFA and determined pK_a values

$c(\text{TFA})$ [mol·L ⁻¹]	pH = pK_a	corrected absorbance $\lambda_{\text{max}} = 385 \text{ nm}$	corrected absorbance $\lambda_{\text{max}} = 340 \text{ nm}$
$7.32 \cdot 10^{-5}$	4.13	0.261	0.509
$1.22 \cdot 10^{-4}$	3.91	0.267	0.496
$2.44 \cdot 10^{-4}$	3.61	0.301	0.479
$6.10 \cdot 10^{-4}$	3.21	0.338	0.420
$8.54 \cdot 10^{-4}$	3.06	0.350	0.385
$1.22 \cdot 10^{-3}$	2.91	0.379	0.366
$1.83 \cdot 10^{-3}$	2.73	0.402	0.345
$3.05 \cdot 10^{-3}$	2.51	0.418	0.314

By plotting the corrected absorbances at 340 and 385 nm against the calculated pH values, the pK_a value of **MEQDMA-H⁺** was obtained (Figure S3). The pH at the intersection between the protonated and the non-protonated species represented identical concentrations and, thus, corresponded to the half-equivalence point of a titration curve. Accordingly, the pK_a accounted to 2.91 for **MEQDMA-H⁺**.

6. Determination of the pK_a of **MEQDMA-H⁺** by fluorescence spectroscopy

The pK_a of **MEQDMA-H⁺** was also be determined by fluorescence spectroscopy assuming a static quenching of the fluorescence by altering the emissive chromophore **MEQDMA** to **MEQDMA-H⁺** in the ground state. As the concentration of TFA increased fluorescence intensity of **MEQDMA** decreased (Figure S4).

Based on the Stern-Volmer equation 5, the quotient of the emission intensity in the absence of the quencher (TFA) F_0 and the emission intensity after addition of the quencher (TFA) F was plotted against the concentration of trifluoroacetic acid (Table 5).

$$\frac{F_0}{F} = 1 + K_{sv}[Q] \quad (5)$$

Table 5. The concentrations of the respective TFA solution and the determined quotient $F_0 \cdot F^{-1}$

$c(\text{TFA})$ [mol·L ⁻¹]	$F_0 \cdot F^{-1}$
$1.83 \cdot 10^{-4}$	4.13
$2.56 \cdot 10^{-4}$	3.91
$3.29 \cdot 10^{-4}$	3.61
$7.32 \cdot 10^{-4}$	3.21
$1.10 \cdot 10^{-3}$	3.06
$1.22 \cdot 10^{-3}$	2.91

The resulting linear correlation from equation 6 from Figure S4 provided the Stern-Volmer constant K_{sv} (slope), y-axis intercept and correlation coefficient r^2 . The Stern-Volmer constant K_{sv} in the Stern-Volmer equation provided the position of the chemical equilibrium. Using the linear correlation, the concentration of the quencher was determined. In this case, K_{sv} equaled K_a .

$$\frac{F_0}{F} = 0.7972 + 1186.58 [H^+] \quad (r^2 = 0.99) \quad (6)$$

The pK_a value of **MEQDMA-H⁺** was determined for both absorption and fluorescence spectroscopy with values of 2.9 (UV/Vis) and 3.1 (fluorescence), respectively. The pK_a value of **MEQDMA-H⁺** was determined for both absorption and fluorescence spectroscopy, with values of 2.9 (UV/Vis) and 3.1 (fluorescence), respectively.

7. Difference spectra and Job plots of Sc(OTf)₃ and MEQDMA in ethyl acetate and acetonitrile

For complexation studies of **MEQDMA** and various metal triflates first a stock solution of **MEQDMA** (1 mg) in a volumetric flask (25 mL) filled with the corresponding solvent was prepared. Then, stock solutions of Sc(OTf)₃ (1.30 mg) in the corresponding solvents were prepared. For maintaining constant overall concentration for the Job measurements aliquots of the stock solutions of Sc(OTf)₃ and of **MEQDMA** were combined to give the corresponding mole fractions of **MEQDMA** (Table 6).

Table 6. Mole fractions of **MEQDMA** maintaining a constant overall concentration and volume from volumes of **MEQDMA** and Sc(OTf)₃ stock solutions

V(MEQDMA)	V(Sc(OTf) ₃)	X(MEQDMA)
1.0 mL	0.0 mL	1.0
0.9 mL	0.1 mL	0.9
0.8 mL	0.2 mL	0.8
0.7 mL	0.3 mL	0.7
0.6 mL	0.4 mL	0.6
0.5 mL	0.5 mL	0.5
0.4 mL	0.6 mL	0.4
0.3 mL	0.7 mL	0.3
0.2 mL	0.8 mL	0.2
0.1 mL	0.9 mL	0.1
0.0 mL	1.0 mL	0.0

The isosbestic points were obtained from a titration experiment. The difference spectra of titration experiments are depicted in Figures S6 (ethyl acetate) and S8 (acetonitrile) and the Job plots are shown in Figures S7 (ethyl acetate) and S9 (acetonitrile). The absorption maximum at 384 nm illustrates the increase in ML complex, it while the absorption minimum at 415 nm indicates the decrease in free ligand **MEQDMA** (Figure S10).

8. Aggregation-induced emission of MEQDMA in isopropanol/water and acetonitrile/water

For AIE experiments first a stock solution of **MEQDMA** (1 mg) in a volumetric flask (25 mL) filled with the corresponding solvent was prepared. For each measurement, an aliquot of the stock solution (0.1 mL for isopropanol/water; 0.2 mL for acetonitrile/water) was placed into a 10 mL volumetric flask and diluted with the solvent or the respective volume fractions of deionized water (20, 45, 60, 85, 95 and 99% for isopropanol/water, Figure S11; 4, 50, 70, 95, and 99% for acetonitrile/water, Figure S12). For each measurement 3 mL of the corresponding solution was transferred into the cuvette.

Acknowledgements

The authors cordially thank the Fonds der Chemischen Industrie and the Deutsche Forschungsgemeinschaft (Mu 1088/9-1) for financial support.

Supplementary Material

The supplementary material file contains UV/Vis spectra for the determination of the pK_a of **MEQDMA-H⁺**, fluorescence spectra for the determination of the pK_a of **MEQDMA-H⁺**, difference UV/Vis spectra and Job plots of Sc(OTf)₃ and MEQDMA in ethyl acetate and acetonitrile, and aggregation-induced emission spectra of **MEQDMA** in isopropanol/water and acetonitrile/water.

References

1. Mamedov, V. A. *Quinoxalines*. Springer, Cham. 2016.
<https://doi.org/10.1007/978-3-319-29773-6>
2. Chawla, G. ; Gupta, O.; Pradhan, T. *ChemistrySelect* **2023**, *8*, e202301401
<https://doi.org/10.1002/slct.202301401>
3. Pereira, J. A.; Pessoa, A. M.; Cordeiro, M. N. D. S.; Fernandes, R.; Prudencio, C.; Noronha, J. P.; Vieira, M. *Eur. J. Med. Chem.* **2015**, *97*, 664-672.
<https://doi.org/10.1016/j.ejmech.2014.06.058>
4. Tariq, S.; Somakala, K.; Amir, M. Quinoxaline: An insight into the recent pharmacological advances. *Eur. J. Med. Chem.* **2018**, *143*, 542-557.
<https://doi.org/10.1016/j.ejmech.2017.11.064>
5. Montana, M.; Montero, V.; Khoumeri, O.; Vanelle, P. *Molecules* **2020**, *25*, 2784.
<https://doi.org/10.3390/molecules25122784>
6. Pinheiro, C. A. ; Mendonça Nogueira, T. C.; de Souza, V. N. M. *Anti-Cancer Agents Med. Chem.* **2016**, *16*, 1339-1352.
<https://dx.doi.org/10.2174/1871520616666160622090839>
7. Montana, M.; Mathias, F.; Terme, T.; Vanelle, P. *Eur. J. Med. Chem.* **2019**, *163*, 136-147.
<https://doi.org/10.1016/j.ejmech.2018.11.059>
8. Albert, A. in: A. R. Katritzky, Ed, *Physical Methods in Heterocyclic Chemistry*, Vol 1, Chpt 1. Academic Press: New York, 1963.
9. Achelle, S.; Baudequin, C.; Ple, N. *Dyes Pigm.* **2013**, *98*, 575-600.
<https://doi.org/10.1016/j.ejmech.2014.06.058>
10. Liu, M.; Gao, Y.; Zhang, Y.; Liu, Z.; Zhao, L. *Polym. Chem.* **2017**, *8*, 4613-4636.
<https://doi.org/10.1039/C7PY00850C>
11. Zhou, L.; Chen, J. X.; Ji, S.; Chen, W. C.; Huo, Y. *Acta Chimica Sinica* **2022**, *80*, 359-372.
<https://doi.org/10.6023/A21120587>
12. da Silva, L. C.; Machado, V. G.; Menezes, F. G. *Chem. Pap.* **2021**, *75*, 1775-1793.
<https://doi.org/10.1007/s11696-020-01484-9>
13. Dey, S. K.; Al Kobaisi, M.; Bhosale, S. V. *ChemistryOpen* **2018**, *7*, 934-952.
<https://doi.org/10.1002/open.201800163>
14. Biesen, L.; Müller, T. J. J. in *Handbook of Aggregation-Induced Emission*, B. Z. Tang, Y. Tang, eds., Wiley-VCH Verlag GmbH & Co. KgaA: Weinheim, 2022, Vol. 1, pp 455-484.
15. Cheeseman, G. W. H. *Adv. Heterocycl. Chem.* **1963**, *2*, 203-244.
[https://doi.org/10.1016/S0065-2725\(08\)60750-3](https://doi.org/10.1016/S0065-2725(08)60750-3)
16. Mamedov, V. A. Synthesis of Quinoxalines. In *Quinoxalines*. Springer, Cham. 2016, pp 5–133.

- https://doi.org/10.1007/978-3-319-29773-6_2
17. Yashwantrao, G.; Saha, S. *Org. Chem. Front.* **2021**, *8*, 2820-2862.
<https://doi.org/10.1039/D0QO01575J>
18. Biesen, L.; Müller, T. J. J. *Adv. Synth. Catal.* **2021**, *363*, 980-1006.
<https://doi.org/10.1002/adsc.202001219>
19. Gers, C. F.; Nordmann, J.; Kumru, C.; Frank, W.; Müller, T. J. J. *J. Org. Chem.* **2014**, *79*, 3296-3310.
<https://doi.org/10.1021/jo4025978>
20. Merkt, F. K.; Höwedes, S. P.; Gers-Panther, C. F.; Gruber, I.; Janiak, C.; Müller, T. J. J. *Chem. Eur. J.* **2018**, *24*, 8114-8125.
<https://doi.org/10.1002/chem.201800079>
21. Merkul, E.; Dohe, J.; Gers, C.; Rominger, F.; Müller, T. J. J. *Angew. Chem. Int. Ed.* **2011**, *50*, 2966-2969.
<https://doi.org/10.1002/anie.201007194>
22. Merkt, F. K.; Müller, T. J. J. *Sci. China Chem.* **2018**, *61*, 909-924.
<https://doi.org/10.1007/s11426-018-9295-4>
23. Lindic, M. M.; Zajonz, M.; Gers-Panther, C.; Müller, T. J. J.; Schmitt, M. *Spectrochim. Acta A* **2020**, *228*, 117574.
<https://doi.org/10.1016/j.saa.2019.117574>
24. Gers-Panther, C. F.; Fischer, H.; Nordmann, J.; Seiler, T.; Behnke, T.; Würth, C.; Frank, W.; Resch-Genger, U.; Müller, T. J. J. *J. Org. Chem.* **2017**, *82*, 567-578.
<https://doi.org/10.1021/acs.joc.6b02581>
25. Nirmalanathan, N.; Behnke, T.; Hoffmann, K.; Kage, D.; Gers-Panther, C. F.; Frank, W.; Müller, T. J. J.; Resch-Genger, U. *J. Phys. Chem. C* **2018**, *122*, 11119-11127.
<https://doi.org/10.1021/acs.jpcc.8b01425>
26. Merkt, F. K.; Pieper, K.; Klopotoski, M.; Janiak, C.; Müller, T. J. J. *Chem. Eur. J.* **2019**, *25*, 9447-9455.
<https://doi.org/10.1002/chem.201900277>
27. Fery-Forgues, S.; Lavabre, D. *J. Chem. Educ.* **1999**, *76*, 1260-1264.
<https://doi.org/10.1021/ed076p1260>
28. Easter, D. C.; Baronavski, A. P. *Chem. Phys. Lett.* **1993**, *201*, 153-158.
[https://doi.org/10.1016/0009-2614\(93\)85049-T](https://doi.org/10.1016/0009-2614(93)85049-T)
29. Reichardt, C. *Chem. Rev.* **1994**, *94*, 2319-2358.
<https://doi.org/10.1021/cr00032a005>
30. Lippert, E. Z. *Elektrochem.* 1957, *61*, 962-975.
<https://doi.org/10.1002/bbpc.19570610819>
31. Mataga, N.; Kaifu, Y.; Koizumi, M. *Bull. Chem. Soc. Jpn.* **1956**, *29*, 465-470.
<https://doi.org/10.1246/bcsj.29.465>
32. Lakowicz, J. R. *Principles of Fluorescence Spectroscopy*, 3rd ed.; Springer: Berlin/Heidelberg, **2006**; pp 213-216.
<https://doi.org/10.1007/978-0-387-46312-4>
33. Klausen, K. S.; Langmyhr, F. J. *Anal. Chim. Acta*, **1963**, *28*, 335 - 340.
[https://doi.org/10.1016/S0003-2670\(00\)87242-6](https://doi.org/10.1016/S0003-2670(00)87242-6)
34. Renny, J. S.; Tomasevich, L. L.; Tallmadge, E. H.; Collum, D. B. *Angew. Chem. Int. Ed.* **2013**, *52*, 11998-12013.
<https://doi.org/10.1002/anie.201304157>
35. Connors, K. A. *Chem. Rev.* **1997**, *97*, 1325-1358.
<https://doi.org/10.1021/cr960371r>

36. Thordarson, P. *Chem. Soc. Rev.* **2011**, *40*, 1305–1323.

<https://doi.org/10.1039/C0CS00062K>

37. MATLAB Version: 9.1.0.441655 (R2016b) Natick, Massachusetts: The MathWorks Inc.; **2016**.

This paper is an open access article distributed under the terms of the Creative Commons Attribution (CC BY) license (<http://creativecommons.org/licenses/by/4.0/>)